Supporting Information

Strain Relaxation in '2D/2D and 2D/3D Systems': Highly Textured Mica/Bi_2Te_3, Sb_2Te_3/Bi_2Te_3 and Bi_2Te_3/GeTe Heterostructures

Heng Zhang,* Daniel T. Yimam, Sytze de Graaf, Jamo Momand, Paul A. Vermeulen, Yingfen Wei, Beatriz Noheda, and Bart J. Kooi*

Zernike Institute for Advanced Materials
Nijenborgh 4 9747 AG Groningen, The Netherlands
Corresponding author: heng.zhang@rug.nl
Corresponding author: b.j.kooi@rug.nl

Material	a	b	c	Structure	Ref
mica	5.28	-	19.95	Monoclinic (C2/c)	Our results
Bi_2Te_3	4.395	4.395	30.44	Trigonal (R-3m)	1
GeTe	4.189	4.189	10.65	Trigonal (R3m)	2
Sb_2Te_3	4.264	4.264	30.458	Trigonal (R-3m)	3

Table S1 The lattice parameters (in Angstrom) and crystal structures of the materials used in our work.

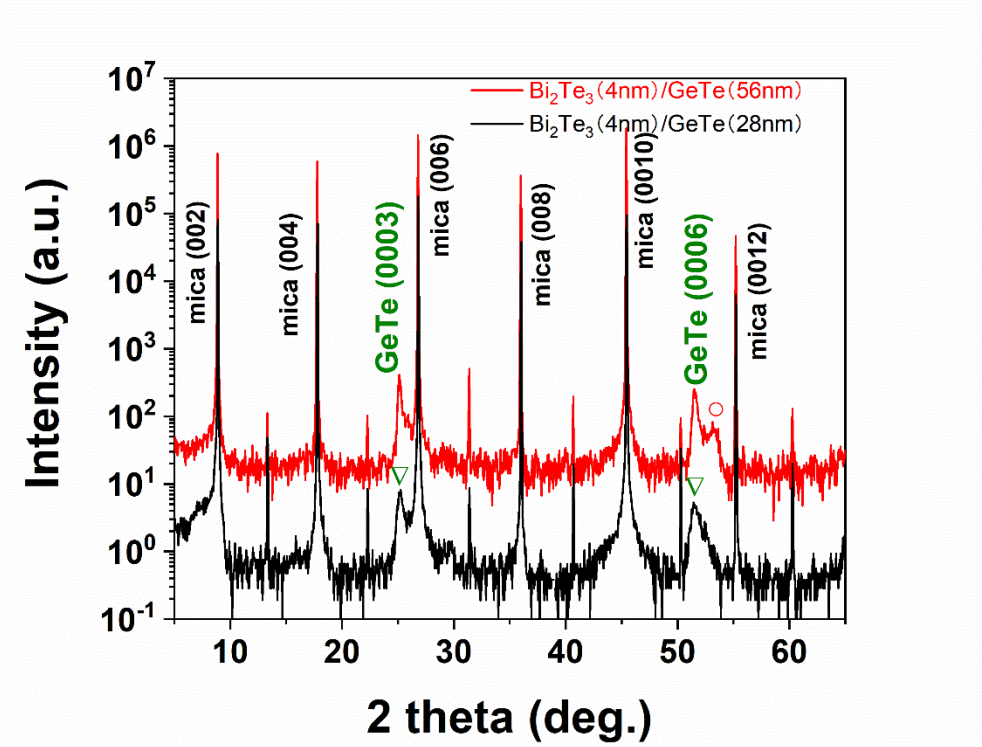

Figure S1. Specular θ-2θ XRD patterns of mica/Bi_2Te_3/GeTe heterostructure films in the range of 5° - 65°: 28 nm GeTe (black) and 56 nm GeTe (red) on the top of 4 nm Bi_2Te_3.

Relatively large 2θ-range XRD curves are shown in Figure S1. As can be seen, all the sharp peaks with high intensity commonly reported in literature belong to substrate mica (00L).[4] The pattern for the thin heterostructure only has two broad peaks around 25.1° and 51.5°, corresponding to (0003) and (0006) of α-GeTe, respectively. Absence of diffraction from other crystal planes indicates good c-axis out-of-plane orientation of GeTe on mica. However, in heterostructure with thicker GeTe film, another shoulder peak around 53.3° is present, which can be indexed as GeTe $(04\bar{4}2)$.

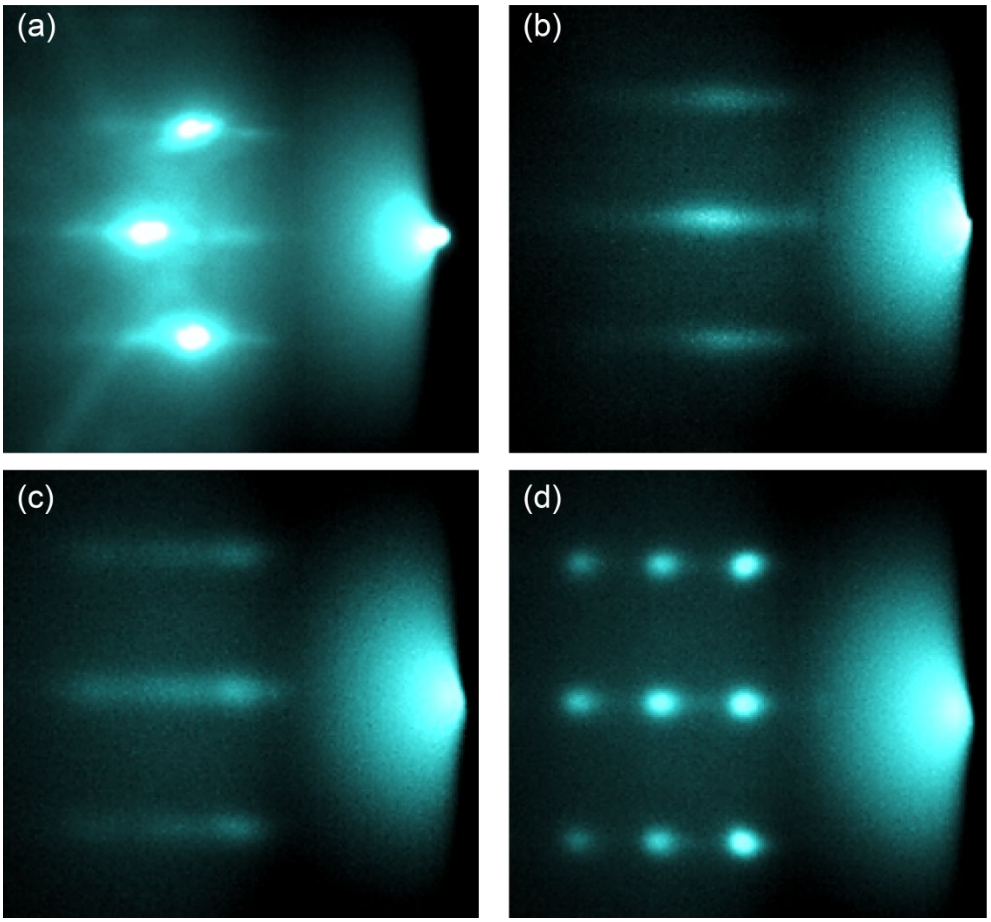

Figure S2. RHEED patterns of (a) the mica substrate, (b) 60 nm of Bi_2Te_3, (c) (4 nm/5 nm) Bi_2Te_3/GeTe and (d) (4 nm/28 nm) Bi_2Te_3/GeTe surfaces. Azimuth: $[1\bar{1}0]$ for mica and $[11\bar{2}0]$ for Bi_2Te_3 and GeTe.

Figure S2a shows the typical dots pattern of cleaved mica surface obtained by *in-situ* reflection high-energy electron diffraction (RHEED) with an azimuth parallel to $[1\bar{1}0]$ axis.[5] The dots pattern of the smooth mica surface changes quickly to a streaky and sharp pattern at the beginning of Bi_2Te_3 deposition, which signifies a high-quality textured film. This high quality is also confirmed by the smooth surface shown by the AFM image depicted in Figure S3a. One can notice that the RHEED pattern of GeTe sublayer after 5 nm deposition on the top of 4 nm Bi_2Te_3 sublayer still keeps streaky features, but the length of the stripes grow longer and the intensities become weaker. After 5 nm of GeTe growth however, the stripy pattern gradually gives way to dots due to the change from 2D to 3D growth, which causes the increase of roughness. This growth mode is in agreement with the report by Stranski *et al*.[6]

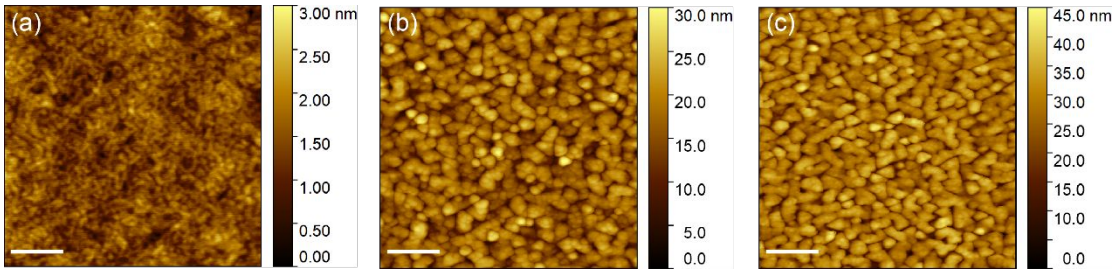

Figure S3. AFM tapping mode images of (a) 60 nm Bi_2Te_3, (b) (4 nm/28 nm)Bi_2Te_3/GeTe heterostructure film and (c) (4 nm/56 nm)Bi_2Te_3/GeTe heterostructure film. The scale bars in the three images are 200 nm.

Atomic force microscope (AFM) images visually show the surface topography of our films. It is difficult to calculate the domain size within the Bi_2Te_3 film on mica because the domain boundaries are expected to be of low-angle type and the surface is quite smooth. The GeTe elliptical domains, separated by valleys, have sizes up to ~80 nm. The root mean square roughness (RMS) of Bi_2Te_3 film is ~0.3 nm. For comparison, 28 nm and 56 nm GeTe are grown on the top of 4 nm Bi_2Te_3 sublayer. We found that with the increase of GeTe sublayer the determined RMS roughness increased from ~4 nm to ~6 nm, which is comparable with the roughness of 3D GeTe films grown by the MBE method.[7]

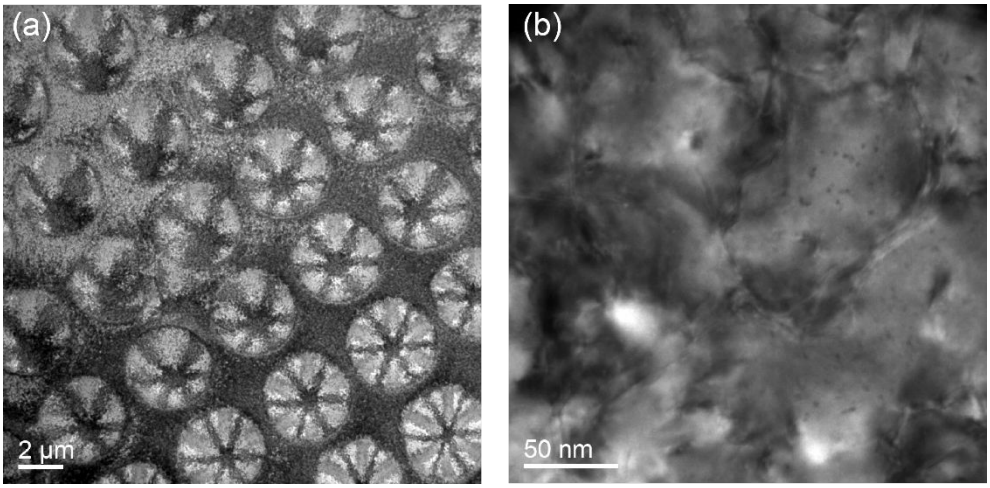

Figure S4. (a) Bright field plan-view TEM image of 60nm Bi_2Te_3 film (as floated off from mica substrate) on Quantifoil grid. (b) High magnification bright field TEM image in the center of a hole of the Quantifoil grid showing (low angle) grain boundaries in the Bi_2Te_3 film.

A 60 nm Bi_2Te_3 film as grown on mica is floated off and captured on a Quantifoil grid. In overview bright-field TEM images of this film in plan-view orientation reproducible bending contour patterns can be observed in the holes of the Quantifoil grid like shown in Figure S4a. As the holes provide less supporting force to the film, they form a weakly concave bending surface in each hole when we transfer the floated film to the grid. Therefore, a regular bending pattern of the Bi_2Te_3 film occurs in each hole. The six-fold symmetry observed for the bending pattern in each hole nicely demonstrates the highly textured nature of the film with c-axis out-of-plane. A typical high magnification image of 60 nm Bi_2Te_3 film is shown in Figure S4b. Comparing with GeTe film (in Figure S5d), no voids were observed for the Bi_2Te_3 film. One should notice that (low-angle) domain boundaries are observed in the image, which means that the Bi_2Te_3 film is not truly single crystal even though distinct ‘single crystalline’ RHEED patterns can be observed with different azimuth.

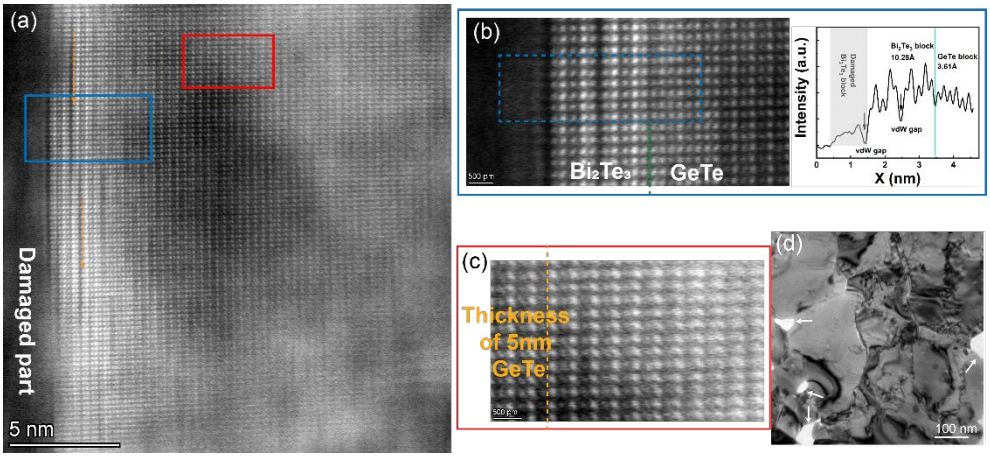

Figure S5. (a) Overview HAADF-STEM image of cross-sectional 28 nm GeTe heterostructure film (on 4 nm Bi_2Te_3 on mica). The orange arrows indicate bilayer defects present in the Bi_2Te_3 seed layer. (b) A magnified image of the blue rectangle area shown in (a) with the corresponding HAADF intensity line-scan where the interfaces mica/ Bi_2Te_3 and Bi_2Te_3/GeTe can be distinguished. The green line in (b) indicates the interface between Bi_2Te_3 sublayer and GeTe sublayer. (c) A magnified image of GeTe layer when reaching a thickness of 5 nm on top of Bi_2Te_3 (red rectangle area in (a)). (d) Bright field plan-view image of this heterostructure film. The white arrows indicate voids in the film.

The detailed structure of the mica/(4nm)Bi_2Te_3/(28nm)GeTe heterostructure film is analyzed using HAADF-STEM, of which a cross-sectional overview is shown in Figure S5a. As is well-known, mica is a good substrate for high quality film growth, but quite sensitive to the electron beam of the TEM, creating an obstacle for (S)TEM characterization. At the left edge of the overview image, in the dark area, the atomic structure of mica or film can therefore not be observed. Hence, we deduce that the mica/Bi_2Te_3 interface was damaged by the ion beam during TEM lamella preparation or by the electron beam during imaging. In fact, during viewing of the mica, in order to align it accurately into the zone axis, it becomes amorphous in the area viewed (not shown here). Still, the zone axis alignment allows the Bi_2Te_3 seed layer (the first two quintuple layers) to be clearly visible. In addition, bilayer defects are found in these layers, similar to the ones observed earlier for Sb_2Te_3/GeTe superlattices.[8] An example is highlighted in Figure S5a as confined between the orange vectors. The high-resolution image of the Bi_2Te_3-GeTe interface and corresponding line-scan are shown in Figure S5b. The lateral extension of vdWaals gaps in Bi_2Te_3 quintuple layers, as well as the root mean square (RMS) roughness value of less than 1 nm in thick Bi_2Te_3 film (Figure S3a) confirm that high-quality layer by layer growth of Bi_2Te_3 films is achieved on mica by PLD. Also, perfect Te-Ge bonding at the interface between Bi_2Te_3 and GeTe can be observed. It is measured from the line-scan that both the Bi_2Te_3 quintuple and GeTe bilayer thickness at the interface (10.28 Å and 3.61 Å, respectively) is larger than the bulk value (10.15 Å and 3.55 Å, respectively).[1,2] This can be explained by the fact that beam damage on mica causes some bending of the lamella giving rise to a systematic error in the thickness measurement. This is probably also the reason that the exponentially decaying strain evolution in the GeTe cannot be extracted from the present STEM results. Still, the intensity of Ge and Te atomic columns close to the Bi_2Te_3 quintuples (in the left part of the image) are sharp and distinct while the intensity of columns close to the GeTe surface (in the right part) is non-uniform and obscure, which can be attributed to the GeTe (000L) distorted planes. From Figure S5c it

becomes apparent that this transition starts after about 5 nm growth of GeTe and slowly exacerbates the quality of the out-of-plane texture, in agreement with the streaky and dotty RHEED pattern as presented in Figure S2c and d. This fact again supports the observation that very thin GeTe films, which do not exhibit oblique peaks in the XRD pattern, show a better texture. Thus, it can be deduced that epitaxial GeTe thin films grow *via* a 2D-3D (Stranski-Krastanov) growth mode.[6] Figure S5d shows a typical plan-view image of this Bi_2Te_3/GeTe heterostructure for a GeTe film thickness of 28 nm. The film contains some voids, as seen by the bright spots highlighted by white arrows. This is not observed for Bi_2Te_3 films (Figure S4), which can also be attributed to the different growth modes in these two films (more 2D for Bi_2Te_3 and 3D for GeTe). In spite of sharp interfaces and the highly textured orientation on the mica substrate, the polycrystalline morphology, which are actually domains with small mutual in-plane tilts, are clearly observable in these GeTe films grown on mica (see Figure S5d). Contrary to the GeTe film grown with MBE on Si (111)-H, absence of transrotational domains illustrate the high quality growth of GeTe in the present heterostructure, which is similar to GeTe grown on Si (111)-Sb.[9] Moreover, perfect GeTe crystalline bilayers directly at the onset of the growth can testify this.

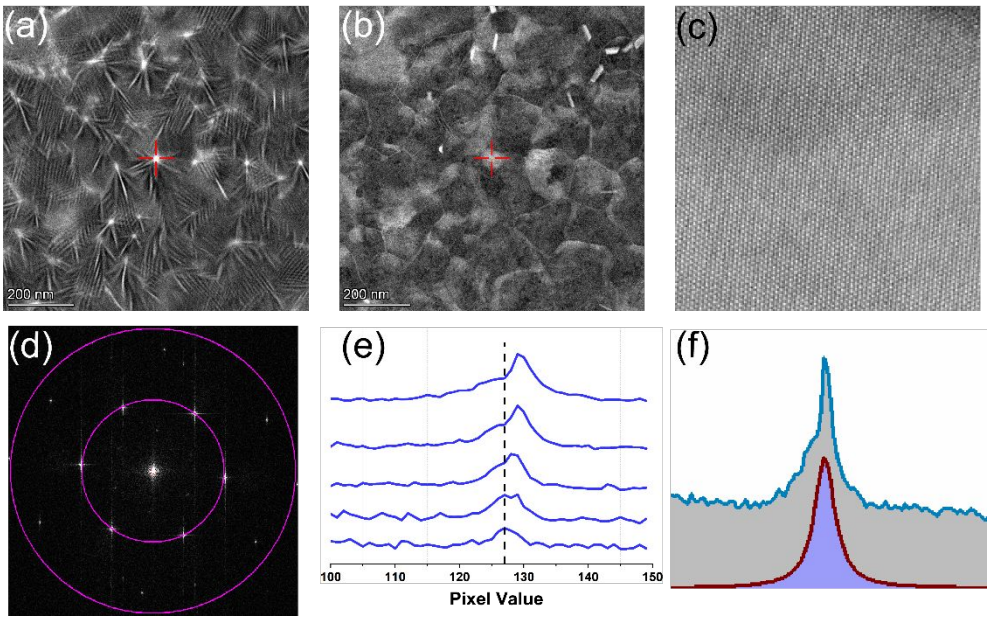

Figure S6. (a) HAADF-STEM visualization of local orientation using an underfocus of ~370 nm. The centers of the star-shaped regions are closest to the zone axis. The region with the red crosshair is selected for imaging. (b) Image from the same region when the film is in focus. The film's crystallites are now clearly observed. It is evident that due to strain relaxation the local zone axis within the crystallite varies. Multiple images were captured by varying the defocus value during imaging which in principle correspond to atomic planes at various depths. (c) An example of an atomic resolution image taken at a defocus of 51 nm. (d) From the high resolution images, the FFTs were extracted and analyzed by a DigitalMicrograph suite of scripts DiffTools[10] with (e) showing the rotation averaging generated intensity profiles. The shift in the intensity profile peaks indicate lattice parameter change for the atomic planes. (f) The intensity profiles were then fitted with a Gaussian function to extract the exact peak locations which were converted to the corresponding a lattice parameter.

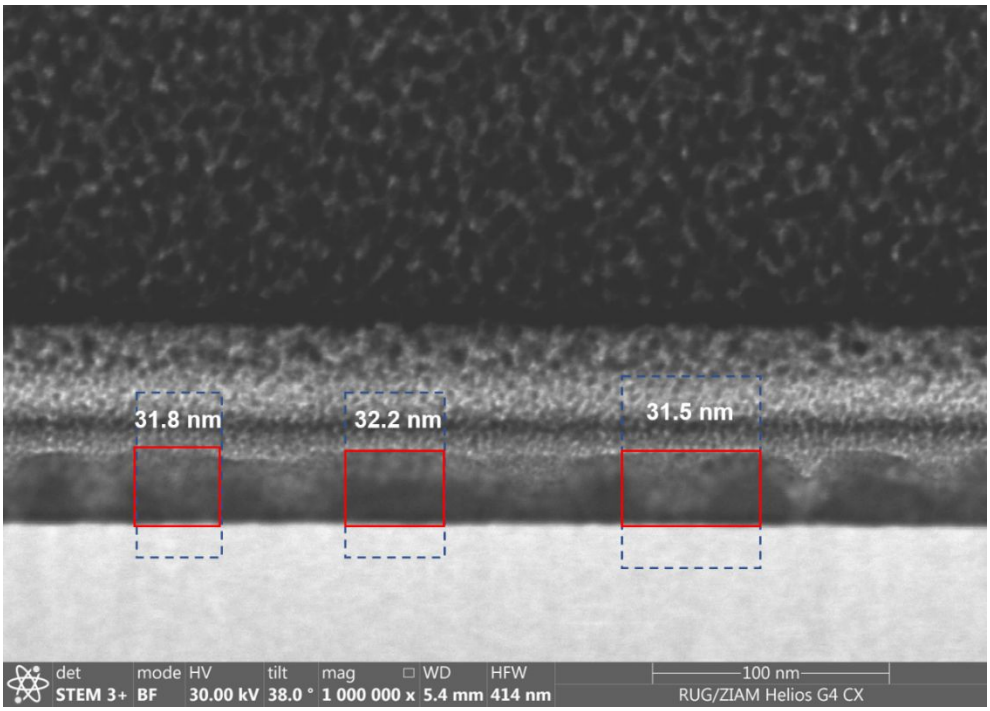

Figure S7. The typical high resolution STEM mode of SEM image of cross-sectional (4 nm/28nm) Bi_2Te_3/GeTe heterostructure. The thicknesses were obtained by taking intensity profile across the film at the different places.

References

1. Chattopadhyay, T.; Boucherle, J., Neutron Diffraction Study on the Structural Phase Transition in GeTe. *J. Phys. C: Solid State Phys.* **1987,** *20*, 1431.
2. Feutelais, Y.; Legendre, B.; Rodier, N.; Agafonov, V., A Study of the Phases in the Bismuth-Tellurium System. *Mater. Res. Bull.* **1993,** *28*, 591-596.
3. Anderson, T.L.; Krause, H.B., Refinement of the Sb2Te3 and Sb2Te2Se Structures and Their Relationship to Nonstoichiometric Sb2Te3-ySey Compounds. *Acta Crystallogr., Sect. B: Struct. Crystallogr. Cryst. Chem.* **1974**, 30, 1307−1310.
4. Richardson, S. M.; Richardson, J. W., Crystal Structure of a Pink Muscovite from Archer's Post, Kenya: Implications for Reverse Pleochroism in Dioctahedral Micas. *Am. Mineral.* **1982,** *67*, 69-75.
5. Gillet, M.; Masek, K.; Potin, V.; Bruyère, S.; Domenichini, B.; Bourgeois, S.; Gillet, E.; Matolin, V., An Epitaxial Hexagonal Tungsten Bronze as Precursor for Wo3 Nanorods on Mica. *J. Cryst. Growth* **2008,** *310*, 3318-3324.
6. Stranski, I. N.; Krastanow, L., Zur Theorie der Orientierten Ausscheidung von Ionenkristallen Aufeinander. *Monatshefte Chem. Verwandte Teile Anderer Wissenschaften* **1937,** *71*, 351-364.
7. Hilmi, I.; Lotnyk, A.; Gerlach, J. W.; Schumacher, P.; Rauschenbach, B., Influence of Substrate Dimensionality on the Growth Mode of Epitaxial 3D-Bonded GeTe Thin Films: From 3D to 2D Growth. *Mater. Des.* **2019,** *168*, 107657.
8. Momand, J.; Wang, R.; Boschker, J. E.; Verheijen, M. A.; Calarco, R.; Kooi, B. J., Interface Formation of Two- and Three-Dimensionally Bonded Materials in the Case of GeTe-Sb2Te3 Superlattices. *Nanoscale* **2015,** *7*, 19136-19143.
9. Momand, J.; Boschker, J. E.; Wang, R.; Calarco, R.; Kooi, B. J., Tailoring the Epitaxy of Sb2Te3 and GeTe Thin Films Using Surface Passivation. *CrystEngComm* **2018,** *20*, 340-347.
10. Mitchell, D. R. G., DiffTools: Software Tools for Electron Diffraction in DigitalMicrograph. *Microscopy Res. and Technique*, **2008,** *71,* 588-593.